LBL-30211

Lawrence Berkeley Laboratory
UNIVERSITY OF CALIFORNIA

Materials & Chemical Sciences Division

Presented at the 12th International Conference on Atomic Physics, Ann Arbor, Michigan, July 29–August 3, 1990, and to be published in the Proceedings

A New Experimental Limit on the Electric Dipole Moment of the Electron

C. Carlberg, K. Abdullah, E.D. Commins, H. Gould, and S.B. Ross

December 1990

U. C. Lawrence Berkeley Laboratory
Library, Berkeley

FOR REFERENCE

Not to be taken from this room

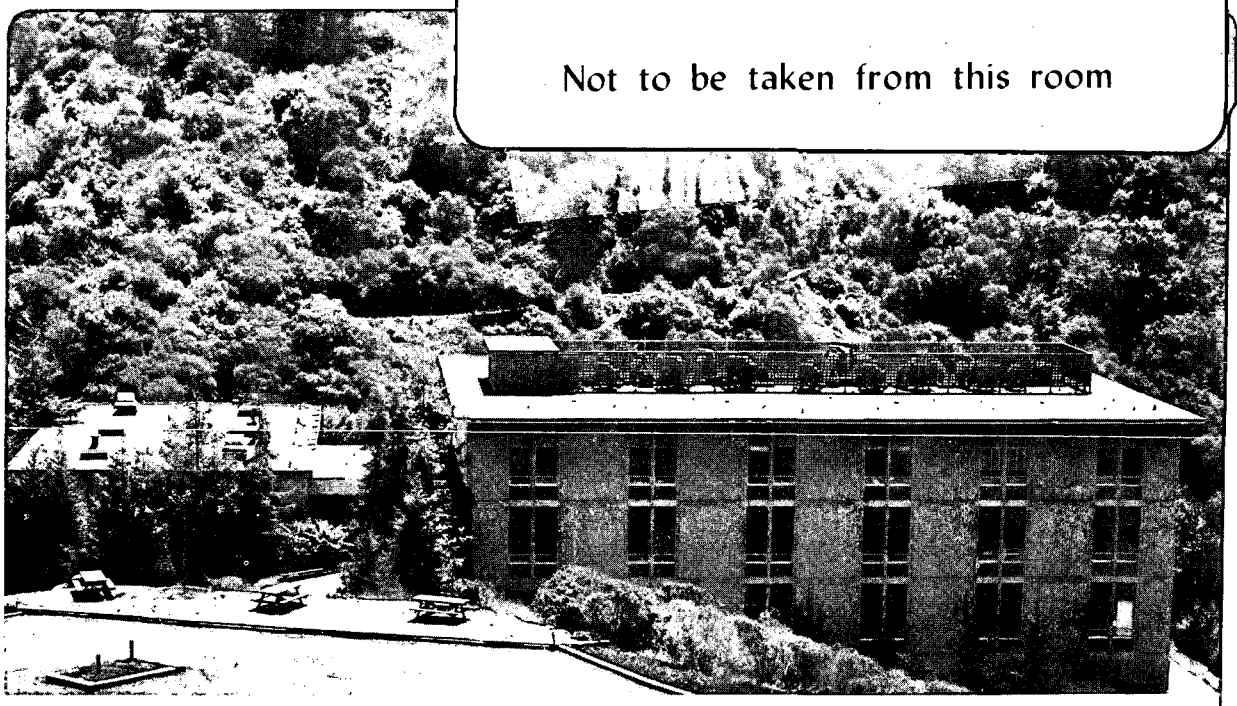

LBL-30211
Copy 1
Bldg. 50 Library.

Prepared for the U.S. Department of Energy under Contract Number DE-AC03-76SF00098

DISCLAIMER

This document was prepared as an account of work sponsored by the United States Government. While this document is believed to contain correct information, neither the United States Government nor any agency thereof, nor the Regents of the University of California, nor any of their employees, makes any warranty, express or implied, or assumes any legal responsibility for the accuracy, completeness, or usefulness of any information, apparatus, product, or process disclosed, or represents that its use would not infringe privately owned rights. Reference herein to any specific commercial product, process, or service by its trade name, trademark, manufacturer, or otherwise, does not necessarily constitute or imply its endorsement, recommendation, or favoring by the United States Government or any agency thereof, or the Regents of the University of California. The views and opinions of authors expressed herein do not necessarily state or reflect those of the United States Government or any agency thereof or the Regents of the University of California.

LBL-30211

A New Experimental Limit on the Electric Dipole Moment of the Electron

C. Carlberg and H. Gould

Materials and Chemical Sciences Division
Lawrence Berkeley Laboratory
University of California
Berkeley, California 94720

K. Abdullah, E.D. Commins, and S.B. Ross

Department of Physics
University of California
and
Materials and Chemical Sciences Division
Lawrence Berkeley Laboratory
University of California
Berkeley, California 94720

December 1990

This work was supported by the Director, Office of Energy Research, Office of Basic Energy Sciences, Chemical Sciences Division; and in part by the Office of High Energy and Nuclear Physics, Division of High Energy Physics and Division of Nuclear Physics, of the U.S. Department of Energy under Contract No. DE-AC03-76SF00098.

A NEW EXPERIMENTAL LIMIT ON THE ELECTRIC DIPOLE MOMENT OF THE ELECTRON

C.Carlberg[1,a], K. Abdullah[1,2,b], E.D.Commins[1,2], H. Gould[1], and S.B. Ross[1,2]
[1]Materials and Chemical Sciences Division
Lawrence Berkeley Laboratory
University of California
Berkeley, California 94720
and
[2]Department of Physics
University of California
Berkeley, California 94720

ABSTRACT

We describe a search for the electric dipole moment d_e of the electron, carried out with ^{205}Tl atoms in the ground state. The experiment makes use of the separated-oscillating-field magnetic-resonance method, laser state selection, fluorescence detection, and two counter-propagating atomic beams. Very careful attention is paid to systematic effects. The result for the atomic electric dipole moment is $d_a=(1.6\pm5.0)\times10^{-24}$ e cm. If we assume the theoretical ratio $d_a/d_e=-600$, this yields $d_e= (-2.7 \pm 8.3)\times10^{-27}$ e cm.

1. INTRODUCTION

We have carried out a new search for the electric dipole moment (EDM) of the electron, a moment that can exist only by virtue of an interaction that violates parity (P) and time reversal invariance (T). The present investigation is thus of interest in connection with CP violation. Indeed, a number of theoretical models of CP violation have recently appeared[1-4] that predict the existence of an electron EDM in the range 10^{-26} -10^{-27} e cm, possibly large enough to be detected in a practical experiment.

The general idea in any EDM search is to detect a dipole moment **d** by measuring its energy W in an electric field **E**:

$$W = -\mathbf{d}\bullet\mathbf{E} \tag{1}$$

but obviously this cannot be done with free electrons, which are charged. One thinks instead about an unpaired valence electron in a neutral atom. The question arises: can the atom as a whole possess an EDM d_a proportional to the electron EDM d_e? Schiff's theorem[5], based on non-relativistic quantum mechanics, states that, to first order in d_e, d_a is zero. However, relativistic effects are important in atoms with large atomic number, and the ratio $R=d_a/d_e$, roughly proportional to $Z^3\alpha^2$, can in fact be much larger than unity[6]. Thus, we actually search for d_a in the $6^2P_{1/2}$ ground state of

thallium (Z = 81), where R is estimated[7-10] to be approximately -600, and interpret the result in terms of d_e.

2. EXPERIMENTAL METHOD

2.1 Thallium Atomic Beams

Our experiment utilizes two vertical atomic beams of thallium, one travelling upward and the other downward (see Fig. 1). This specific feature of a pair of beams with opposite velocities is essential: it permits virtually complete elimination of an important systematic effect: that associated with the interaction of the atomic magnetic moment with the motional magnetic field Exv/c; (see Sec. 4.2). The beams are generated in conventional stainless steel ovens that operate at about 1050°K. The beam velocity distributions closely approximate v^3 Maxwellians, but the beams effuse from rather deep rectangular source slits. Thus their effective temperatures are about 1500°K, corresponding to most-probable velocities of about 4.3×10^4 cm/s. The beam trajectories are defined by various collimating slits to be described below, and are vertical rather than horizontal to avoid deflection from falling in the earth's gravitational field. The measurements are performed on one atomic beam at a time with two computer controlled beam stops switching between them.

2.2 State Selection

Let us follow the progress of the upward-going beam in Fig. 1. After emerging from the oven, and moving in the positive x direction, this beam intersects a cw laser beam directed along y and with linear polarization along z in the state selector region. Note that the entire experiment from here on takes place in a nominally uniform magnetic field B_z, typically .26 Gauss or less, in the z direction. The laser is tuned to the allowed E1 transition $6^2P_{1/2}(F=1) \rightarrow 7^2S_{1/2}(F=1)$ at 378 nm (See Fig. 2). Ground state atoms with $m_F = \pm 1$ can make the optical transition, but the matrix element for $F=1, m_F=0 \rightarrow F=1, m_F=0$ is zero. Atoms excited to the 7S state decay rapidly by spontaneous emission to $6P_{1/2}$ or to $6P_{3/2}$ (with fluorescence at 535 nm); the branching ratio being about 50%. Furthermore, the $6P_{3/2}$ state has a lifetime much longer than the beam flight time through the apparatus. Consequently optical pumping depopulates the ground state components F=1, $m_F=\pm 1$, and increases the population of $F=1, m_F=0$ (by a factor of 1.4). As F=1 atoms leave the state selector they are thus in the pure state $m_F=0$, represented by:

$$\psi = \begin{pmatrix} 0 \\ 1 \\ 0 \end{pmatrix} \tag{2}$$

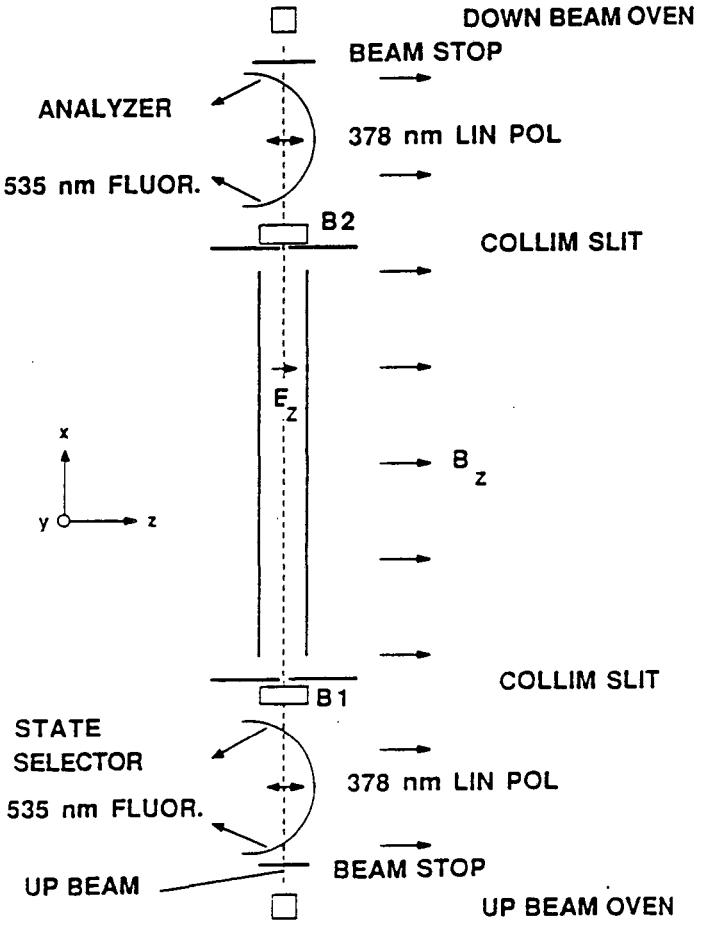

Fig. 1 Schematic diagram of experimental apparatus.

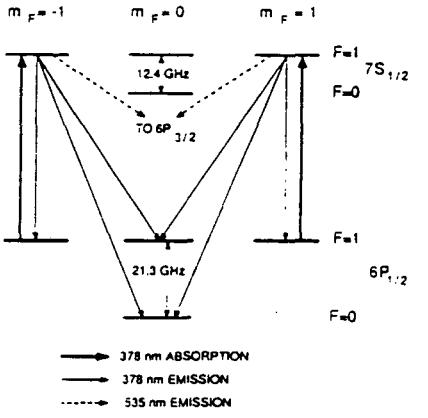

Fig .2 Energy level diagram showing optical state selection scheme.

Further along the atomic beam trajectory is a second optical pumping region identical to the first, called the analyzer. Here also, the atomic beam intersects a beam from the same laser directed along y with linear polarization along z, and tuned to the same transition $6P_{1/2}$, F=1 $\rightarrow$ $7S_{1/2}$, F=1. The analyzer fluorescent signal at 535 nm is proportional to the sum of the populations of F=1,m_F=±1 atoms that enter this region. The laser beam-atomic beam intersection in the state selector or analyzer occurs at the focus of a large reflecting ellipsoid with its axis of revolution along z. Its purpose is to collect 535 nm fluorescence and focus it through a light pipe/optical filter system into a photomultiplier tube.

Fig. 3 shows the state selector fluorescent signal versus laser frequency in the neighborhood of the F=1$\rightarrow$F=1 resonance, and shows that the two naturally occurring thallium isotopes A=203, 205 (with abundances 30%, 70%) are resolved by the isotope shift. All our EDM measurements are carried out with the more abundant isotope A=205.

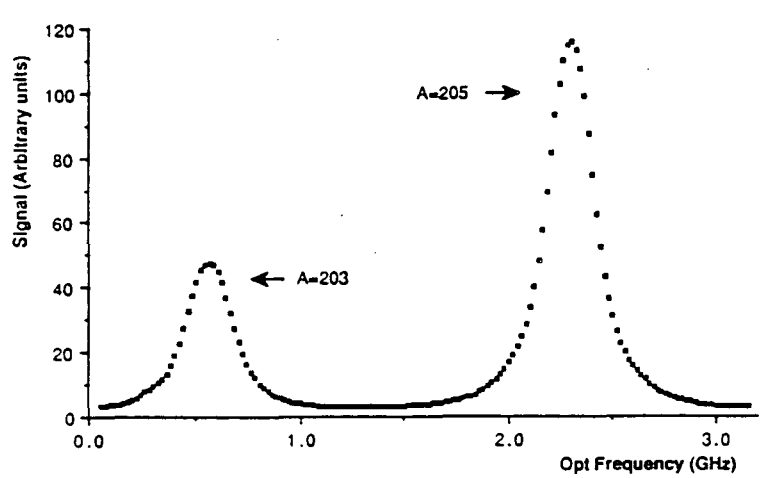

Fig. 3 Fluorescent signal at 535 nm in state selector versus optical frequency, for the F=1$\rightarrow$F=1 378nm transition in isotopes A=203, A=205.

Fig. 4 is a plot of state selector and analyzer fluorescent signals (with different gains) on the A=205 1$\rightarrow$1 line and with no reorientation in the region between state selector and analyzer. The shape of the analyzer signal, in particular the flat bottom of the curve at resonance, is easy to understand: in the polarizer, all m_F = ±1 ground state atoms are removed, and thus there are no m_F=±1 atoms entering the analyzer to generate a fluorescent signal at resonance. Such a signal will only occur if the F=1 state is reoriented (by rf and electric field) in the intervening space. Note also the optical linewidth: it is much broader than the natural width of 21 MHz, because of optical power

broadening (saturation).

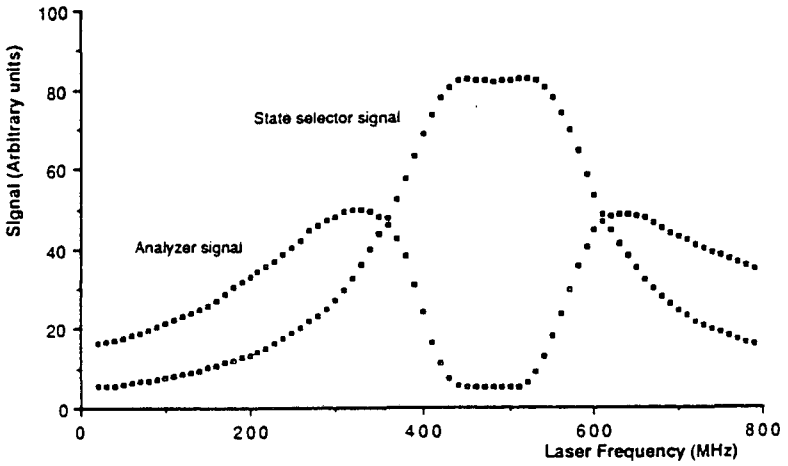

Fig. 4 Fluorescent signals at 535 nm in state selector and analyzer (with different gains) versus optical frequency, for the F=1→F=1 378 nm transition, A=205.

The state selector for the up-going beam serves as the analyzer for the down-going beam, and vice versa.

The 378 nm light is supplied by a Coherent CR 699-21 dye laser with intra-cavity doubling ($LiIO_3$ crystal), pumped by a Coherent 100- K3 Krypton laser. Typically we obtain about 2-3 mW of single mode 378 nm optical power.

2.3 Radio frequency transitions.

Let us continue to follow the upgoing beam after it leaves the state selector (Fig.1). Before reaching the analyzer it passes through two separated rf magnetic fields B_1,B_2 (Ramsey Method)[11] and, in the space between them, an electric field E (typically 100 kV/cm) in the z direction and a pair of collimating slits C_1, C_2. Each rf region has length a=5 cm , and B_1, B_2 oscillate coherently in the x direction with frequency ω near the resonant frequency ω_0 for the transitions F=1, m_F=0 - m_F=±1 in constant magnetic field B_z. B_2 leads B_1 by phase α, which is $\pm\pi/4$ or $\pm 3\pi/4$. The collimating slit dimensions are 0.5 cm x 0.05 cm in the y and z dimensions respectively.

In B_1 the pure F=1, m_F=0 state is converted to a coherent superposition of m_F states. For an atom with velocity v, and at resonance, one finds that in the rotating frame the wave function immediately after the first rf region has changed from (2) to:

$$\psi = \begin{pmatrix} \frac{-i\sigma}{\sqrt{2}} \\ \eta \\ \frac{-i\sigma}{\sqrt{2}} \end{pmatrix} \tag{3}$$

where

$$\sigma = \sin\frac{\gamma B_1 a}{2v}, \qquad \eta = \sqrt{1 - \sigma^2}$$

and $\gamma = \frac{|\mu_0| g_F}{\hbar}$. Wave-function (3) evolves further in the electric field region. After the atom passes through the E field, (3) becomes:

$$\psi = \begin{pmatrix} \frac{-i\sigma}{\sqrt{2}} e^{-i\varepsilon} \\ \eta e^{i\phi} \\ \frac{-i\sigma}{\sqrt{2}} e^{i\varepsilon} \end{pmatrix} \tag{4}$$

Here $\phi = \frac{k E^2}{v}$ arises from the hyperfine-induced quadratic Stark shift (about 400 Hz at 100 kv/cm) of $m_F=0$ relative to $m_F=\pm 1$; k is a constant that has been measured and calculated. (Actually there is also a very small hyperfine/Zeeman-induced quadratic Stark shift between $m_F=1$ and $m_F=-1$ levels that is proportional to B_z; however this effect is of negligible importance). The quantity ε is given by:

$$\varepsilon = \varepsilon_0 + \varepsilon' \tag{5}$$

where

$$\varepsilon_0 = -\frac{d_A E}{\hbar}\frac{L}{v} = -\frac{d_e REL}{\hbar v} \tag{6}$$

arises from the EDM, and where ε', also odd in E, arises from systematic effects to be described below.

The wave function is further modified in the second rf region, and it can be shown that near resonance and for equal B_1, B_2 magnitudes the signal in the analyzer-detector is proportional to the following expression:

$$S = \langle A_1 - A_2 \cos^2(\Delta\omega T + \alpha \mp \varepsilon) + A_3 \cos(\Delta\omega T + \alpha \mp \varepsilon)\rangle \tag{7}$$

where $A_1 = 1 - \eta^4$, $A_2 = \sigma^4$, $A_3 = 2\eta^2\sigma^2 \cos\phi$, $\Delta\omega = \omega - \omega_0$, $T = L'/v$ where $L'=120$ cm is the distance between rf regions, the $\mp$ sign is employed for $B_z > 0$ (<0) and $\langle ... \rangle$ indicates an average over the velocity distribution. A formula similar to (7) applies for the down beam, except that since the roles of the two rf regions are reversed, α must be replaced by $\alpha' = -\alpha$. Also, some contributions to ε' have opposite signs for the up and down beams. The signature of an EDM is the appearance in S of an asymmetry proportional to

the P,T-odd rotational invariant **E•B**.

Fig. 5 shows the fluorescent signal in the analyzer plotted as a function of applied rf frequency in the neighborhood of resonance, for $\alpha = \pm 3\pi/4$. These observed "Ramsey interference" curves are in excellent agreement with calculations based on the foregoing discussion. Optical resonance curves such as Fig. 4, and rf resonance curves such as Fig. 5 are frequently scanned in the course of the experiment.

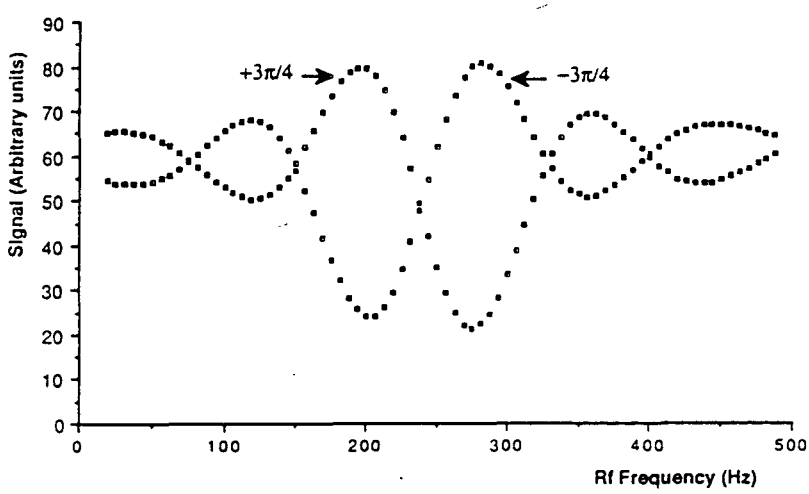

Fig. 5 Fluorescent signal at 535 nm in analyzer versus radio frequency in the vicinity of double loop resonance. Phases $\alpha = \pm 3\pi/4$ are shown.

2.4 Electric Fields

The electric field is produced with a pair of titanium alloy (90% Ti, 6% Al, 4% V) plates, mounted on a structure with plate spacings maintained by precision-ground fused-silica spacers. The plates are 100 cm long, 5 cm wide, and separated by 0.2 cm. Even though they were machined, ground, and assembled with care, there is always a considerable amount of arcing and sparking between the plates when high voltage is first turned on in vacuum. Presumably this happens because of field emission from plate surface irregularities. The effect is reduced by a factor of 10^3 or more by running the plates at high voltage for some hours with argon gas at about 10^{-3} torr pressure. Once the field-emission currents have been reduced by argon treatment, the gas is pumped away, and the plates are ready for service until the next time the system is brought up to atmosphere.

2.5 Magnetic Fields

As mentioned previously, the experiment takes place in a weak, nominally uniform

magnetic field B_z generated by a pair of rectangular coils. In fact the field supplied by these coils is not quite uniform. To produce a Ramsey resonance that is centered on the broad single-loop resonance, we also employ small "trim" coils to generate a correction field B_z' at each rf region. As will be seen below, it is important to cancel the average residual magnetic field B_y at the beam axis. This is accomplished with rectangular coils similar to those for B_z. In addition the system is provided with a set of coils to generate a magnetic field B_x in the beam direction, the purpose of which will be described below. Finally there is a set of four wires (called 'inhomogeneity' wires) parallel to the x axis that can be used in any desired combination to generate magnetic fields that have large gradients in the y and z directions at the beam axis. This entire system of coils and wires, and the vacuum system they surround, are enclosed in a set of four nested magnetic shields (Hypernom and Co-Netic). The magnetic shields have been carefully annealed and are deGaussed with auxiliary deGaussing coils after each change of magnetic field. The shields reduce the ambient magnetic field (from the earth and nearby equipment) by a factor of at least 2×10^4 in the y,z direction and 2×10^3 in the x direction.

3. DATA ACQUISITION

Before we acquire data, the laser frequency is locked to the center of the optical resonance by the computer. The computer then locks the rf synthesizer frequency to the center of the Ramsey resonance. The actual EDM asymmetry search then consists of repeated measurements of fluorescent signals in the analyzing region for different experimental conditions (chops).

In order to determine our sensitivity to an atomic EDM we must measure what frequency shift a certain signal difference corresponds to. Therefore we collect half of our data 1 Hz above the center of double-loop resonance and the other half 1 Hz below. From this known frequency shift and the measured signal difference it is possible to measure the slope of the resonance and thus calibrate the sensitivity. The latter quantity is continuously constructed from the same data that determines the EDM .

In addition to the calibration stepping of the rf frequency there are three more computer controlled chops : 1) The rf phase difference α (rf phase chop), 2) the electric field polarity reversal (E chop) and 3) the up-down beam reversal (beam chop). The rf phase chop minimizes false effects from the quadratic Stark effect and also reduces noise caused by frequency-independent fluctuations such as laser or atomic beam intensity and background variations. Naturally, the purpose of the electric field chop is to extract the true EDM, and it is the only chop which averages noise from magnetic field fluctuations. As mentioned previously, the beam chop largely eliminates the false EDM asymmetry due to the Exv effect.

The rf phase is chopped after each 0.05 s of integration among +45,-45,+135, and -135 degrees. The electric field is reversed after 0.8 s of integration by a computer controlled high voltage switch, the rf frequency (the calibration chop discussed earlier) is stepped after 3.2 s of integration, and the direction of the atomic beam is reversed after 6.4 s of integration. Note that these chops are nested in each other and that, for example, each rf phase is repeated four times for one sign of the electric field. After a change of rf-phase we wait 0.018 s to insure that atoms which have experienced the previous rf-phase have passed through the analyzing region. When the electric field is reversed the experiment pauses for 0.4 s to let the plates charge up completely before continuing the integration. The same delay (0.4 s) is also used for the calibration step and when the direction of the atomic beam is reversed. Each photomultiplier signal is amplified with a preamplifier and then integrated for 0.9 ms by a gated integrator. The output of the integrator is digitized to 12 bits. The computer then stores the result in a temporary storage array.

Since the signal should be constant within a chop configuration, it is possible to calculate an average signal and its standard deviation from data within a configuration. If the standard deviation is too large, all the data within the actual +E/-E period are rejected and the data-acquisition restarted with the first configuration in the actual E-period. Only after a full E-period is successfully completed are the data stored permanently and data-acquisition allowed to start with the next E-period. This rejection occurred only very rarely in actual runs.

Each photomultiplier is alternately exposed to large and small signals because of the beam chop. After a large signal the tube requires a finite amount of time to recover stability; to prevent this from distorting the small signal systematically we permute the chop start configuration and sequence. After eight full beam periods, corresponding to 104.2 sec. of integration and about 4 min. of real time, the acquisition is halted and the current EDM and $\langle B_y/B_z \rangle$ are displayed. The EDM is proportional to the sum of the up and down beam asymmetries while $\langle B_y/B_z \rangle$ is proportional to the difference. (The latter arises from the motional magnetic field effect discussed in Sec. 4.2). Then B_y is corrected (if necessary) to make $\langle B_y/B_z \rangle$ as small as possible and the center of the optical resonance is redetermined before data acquisition is restarted. After a set of sixteen EDM's are measured an average EDM and its standard deviation are calculated. This result is a data point which represents 26 min. of integration and about 1 hour of real time. Our data points are shown in Fig. 6a,b.

When a data point is completed the current to the magnetic field coils is reversed and/or the electric field cables are reversed manually. The purpose of these reversals is to distinguish between odd and even effects under B and/or E reversal. These reversals also allow us to isolate false effects caused, for example, by computer control signals and the electric field switch. Our overall data taking efficiency was about 30% when taking

into account time needed for waits, rejections, reversals, stabilisations and maintenance.

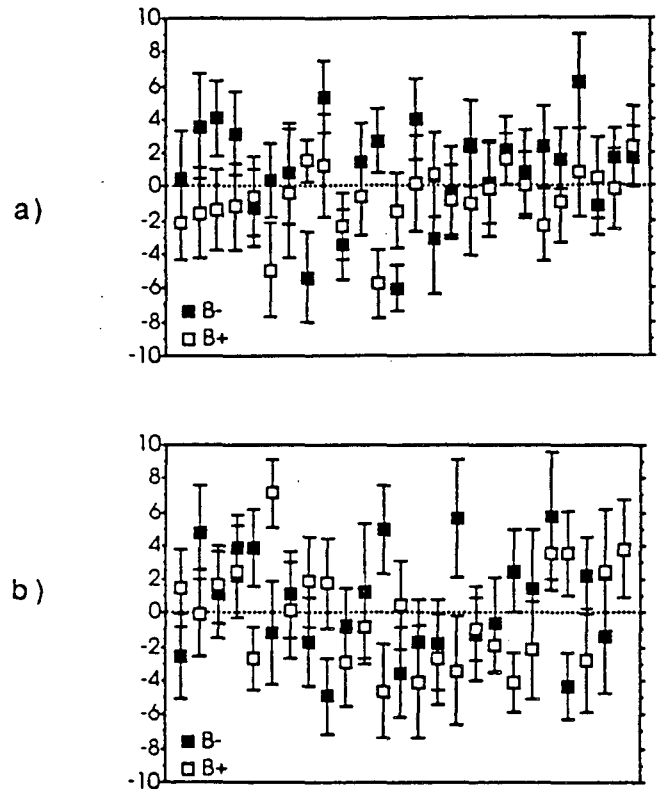

Fig. 6. a) Atomic EDM data of run I. b) Atomic EDM data of run II. In each case the signs of B_- data points are reversed for comparison with B_+ data points. Vertical scale units:10^{-23} e cm.

4. SYSTEMATICS

Isolation and elimination of systematic errors is of central importance in an experiment such as this one, where an extremely small or zero effect is being measured. In the following section we describe in some detail our principal sources of systematic error, and the auxiliary measurements we have carried out to determine them.

4.1 The Geometric Phase Effect

This effect is purely classical, although it requires quantum mechanical interference for observation. It arises when a magnetic field B_x exists that assumes different values at the lower and upper ends of the electric field region. It may be understood intuitively by referring to Fig. 7, which illustrates schematically the experimental set-up we actually use to observe the phenomenon.

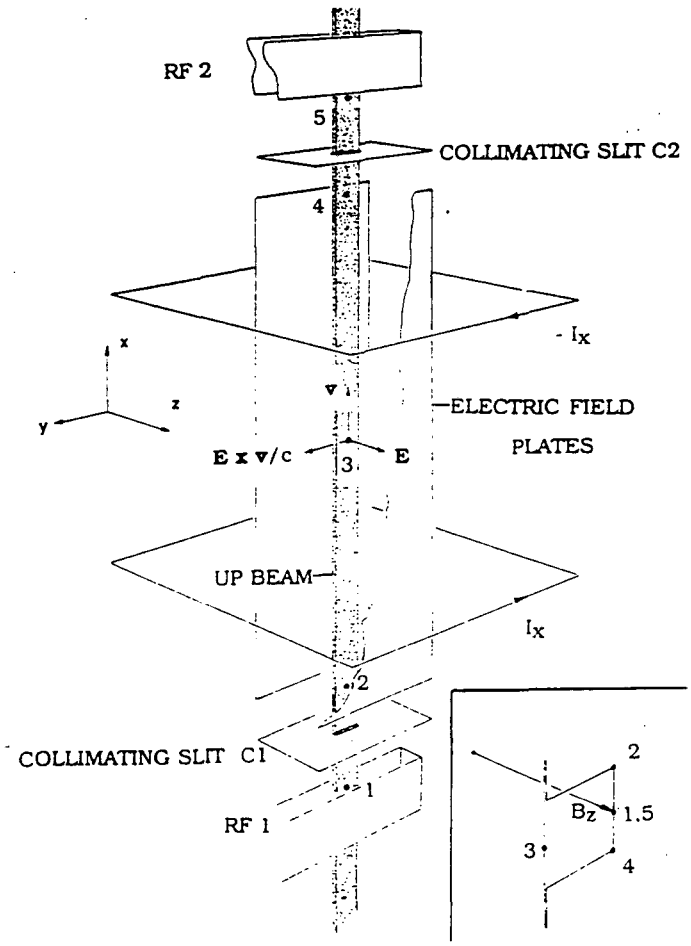

Fig.7 Schematic diagram of experimental setup used to observe the geometric phase effect. Insert shows how tip of magnetic field vector evolves with time.

Fig. 7 shows a pair of x coils with equal and opposite currents I_x for generating a very inhomogeneous field B_x that is positive at the lower end of the electric field region and negative at the upper end. An atom in the up beam at first experiences a negligible field B_x (position # 1). (See also the insert in Fig. 7, which shows the evolution of the tip of B.) As the atom moves closer to the E field region, B_x increases. At the entrance to the electric field B_x is still larger, and the motional field $B_y' = +vE/c$ turns on rapidly but adiabatically(# 2). By this we mean that the magnetic moment precesses many times in the length over which E varies between zero to its full value. As the atom continues to move upward the B_x field continues to increase for a time and then decreases to zero at the midpoint of the E field (#3). B_x continues to decrease until it reaches a mininum where it starts to increase again just before the exit from the electric field.

Here B_x is still negative when B_y' rapidly but adiabatically returns to zero (#4). Then as the atom moves farther upward, B_x returns to zero (#5). It can be seen from the insert to Fig. 7 that the tip of the resultant magnetic field vector describes a closed loop in space, and this yields a contribution to ε' given by the solid angle subtended by **B** as it traces out its path (Berry's phase)[12]. For $|B_z| >> |B_x|, |vE/c|$, this solid angle is just

$$\Omega = \frac{2v(B_{x,1} - B_{x,2})E}{cB_z^2} \tag{8}$$

where $B_{x,1}$ and $B_{x,2}$ refer to the values of B_x at the lower and upper ends of the E field region, respectively.

That this is so can be demonstrated by following the evolution of the F=1 wave-function expressed in terms of "instantaneous" basis states u_1, u_0, u_{-1} , where the quantization axis at any given time is directed along **B**, which is a function of time t in the particle rest frame. We write:

$$\begin{aligned} B_x &= B \sin\theta \cos\varphi \\ B_y &= B \sin\theta \sin\varphi \\ B_z &= B \cos\theta \end{aligned} \tag{9}$$

where B, ϑ, and ϕ depend on t. The basis states are:

$$u_1 = \begin{pmatrix} \frac{1}{2}(1+\cos\theta) \\ \frac{1}{\sqrt{2}}\sin\theta\, e^{i\varphi} \\ \frac{1}{2}(1-\cos\theta)e^{2i\varphi} \end{pmatrix}, \quad u_0 = \begin{pmatrix} -\frac{1}{\sqrt{2}}\sin\theta\, e^{-i\varphi} \\ \cos\theta \\ \frac{1}{\sqrt{2}}\sin\theta e^{i\varphi} \end{pmatrix}, \quad u_{-1} = \begin{pmatrix} \frac{1}{2}(1-\cos\theta)e^{-2i\varphi} \\ \frac{1}{\sqrt{2}}\sin\theta\, e^{-i\varphi} \\ \frac{1}{2}(1+\cos\theta) \end{pmatrix} \tag{10}$$

The wave function :

$$\psi(t) = \sum_{n=-1}^{1} a_n(t)\, u_n(t) \exp\left(-\frac{i}{\hbar}\int_0^t E_n(t')dt'\right) \tag{11}$$

satisfies Schroedinger's equation:

$$H(t)\psi(t) = i\hbar\frac{\partial\psi}{\partial t} \tag{12}$$

where $H=-\mu\bullet\mathbf{B}$. Inserting (11) in (12), multiplying the resulting equations on the left by u_m^*, where m=-1,0,1, and dropping all rapidly oscillating terms, (adiabatic approximation), we obtain:

$$\frac{\dot{a}_m}{a_m} = -\langle u_m | \dot{u}_m \rangle \qquad m = 1,0,-1 \tag{13}$$

Now inserting (10) into (13) we carry out a simple calculation to arrive at:

$$\varepsilon(\text{Geom}) = \int_0^T \dot{\varphi}\,(1-\cos\theta)\,dt \tag{14}$$

and making use of the fact that $|B_z| >> |B_x|,|vE/c|$, we obtain after some simple algebra:

$$\varepsilon(\text{Geom}) = \frac{2v_x(B_{x,1} - B_{x,2})E}{cB_z^2} \tag{15}$$

as expected.

Result (15) is in excellent agreement with observations. It is amusing to note that (15) contains no mention of the Bohr magneton or Planck's constant. However, it was derived in the adiabatic approximation, and if the magnetic moment and/or B_z were sufficiently small or v_x were sufficiently large this approximation would break down. Indeed we have some evidence of such a breakdown from observations of the asymmetry at extremely low B_z.

The quantity ε(Geom) makes a contribution to the EDM asymmetry that is E-odd and B-even if $B_{x,1}$-$B_{x,2}$ reverses when B_z reverses. Indeed we have observed this in auxiliary observations, and our EDM data show evidence of a B-even, E-odd asymmetry that decreases approximately as B_z^{-2}. However there is the possibility of a B-odd contribution as well, if a small non-reversing inhomogeneous field $B_{x,1}$-$B_{x,2}$ exists, (possibly due to the earth's field and that of surrounding equipment) which penetrates the imperfect shield. Note also that inspite of its dependence on v_x, this contribution to the EDM asymmetry would be the <u>same</u> for up and down beams, because $B_{x,1}$-$B_{x,2}$ must also be defined with opposite sign for up and down beams. However, in principle it can be distinguished from the true EDM asymmetry in two ways: first, by its velocity dependence, and second because it varies as B_z^{-2}. In fact, making use of the latter dependence we have been able to set an upper limit to this contribution to d_a of 2.4×10^{-24} e cm for run I and 1.0×10^{-24} e cm for run II. (See Sec.5 for the definition of Runs I and II.)

4.2 The Exv/c Effect

Interaction of the large magnetic moment of the thallium $6^2P_{1/2}$ state with any magnetic field that changes synchronously with the electric field can lead to a systematic asymmetry. The magnetic field includes a motional contribution from the thallium atom's passage through the intense electric field:

$$\mathbf{B}_{mot} = \frac{1}{c}\mathbf{E}\mathbf{x}\mathbf{v} \tag{16}$$

to order v/c. Assuming that the constant electric field defines the z direction, we write:

$$|\mathbf{B}| = \sqrt{B'^2_x + B'^2_y + B'^2_z} \tag{17}$$

where $B'_x = B_x - Ev_y/c$, $B'_y = B_y + Ev_x/c$, $B'_z = B_z$. Since $|v_x| >> |v_y|$ and $|B_z| >> |B_{x,y}|$, (17) may be written as:

$$|B| \approx |B_z| + \frac{B_x^2+B_y^2}{2|B_z|} + \frac{E}{c}\left[v_x\frac{B_y}{|B_z|} - v_y\frac{B_x}{|B_z|}\right] + \frac{v_x^2E^2}{2c^2|B_z|} \tag{18}$$

The third term, linear in electric field, is odd in both E and B, and could yield an EDM-like asymmetry. To a large extent this is eliminated by the use of two opposed beams, since they give an equal and opposite contribution if their velocities are exactly equal and opposite and if they experience the same fields. However, this ideal situation is not achieved exactly. It can be shown that at rf resonance and with a full velocity distribution, the third term in (18) yields a false atomic EDM of:

$$d_a^{False}(Exv) = -3.8\cdot10^{-18}\left\{\left(\overline{v_y}\left\langle\frac{B_x}{B_z}\right\rangle - \overline{v_x}\left\langle\frac{B_y}{B_z}\right\rangle\right)_{up} + \left(\overline{v_y}\left\langle\frac{B_x}{B_z}\right\rangle - \overline{v_x}\left\langle\frac{B_y}{B_z}\right\rangle\right)_{down}\right\} \text{ e cm,} \tag{19}$$

where the velocities are averaged over the velocity distribution and expressed in units of 4.3×10^4 cm/s, while

$$\left\langle\frac{B_{x,y}}{B_z}\right\rangle = \frac{1}{L}\int_0^L \frac{B_{x,y}}{B_z}dx$$

Let:

$$\overline{v}_{x,y\ up} = -\overline{v}_{x,y\ down} + \delta\overline{v}_{x,y}$$

and

$$\left\langle\frac{B_{x,y}}{B_z}\right\rangle_{up} = \left\langle\frac{B_{x,y}}{B_z}\right\rangle_{down} + \frac{\delta B_{x,y}}{\langle B_z\rangle}.$$

Inserting these expressions in (19), and dropping second-order small terms and a very small $v_y\delta B_x/\langle B_z\rangle$contribution, we obtain:

$$d_a^{False}(Exv) = -3.8\cdot10^{-18}\left(\delta\overline{v_y}\left\langle\frac{B_x}{B_z}\right\rangle - \delta\overline{v_x}\left\langle\frac{B_y}{B_z}\right\rangle + \overline{v_x}\frac{\delta B_y}{\langle B_z\rangle}\right) \text{ e cm.} \tag{20}$$

Consider the first term of (20). In the actual experiment, we do not intentionally apply an x field, but the longitudinal magnetic shielding factor is only about 2×10^3, and a residual component B_x of the earth's field is non-zero in the apparatus. In addition, the z and y coils may be tilted and thus generate an x field. Furthermore, although v_y is less than $1 \times 10^{-3}v_x$ we do not measure v_y. However, we can impose a known, large, x field B_{xo} and observe the B-odd false asymmetry. Because the first term of (20) is linear in B_x, the false EDM from this effect during actual runs is reduced by the ratio B_x/B_{xo} . We determine the residual B_x by measuring the rf resonant frequency difference between the up and down beams for $\pm B_{xo}$ and for $B_{xo}=0$. This yields $B_x \approx 2\times10^{-4}$ G. Thus, the possible systematic at 120 kHz was less than 1.3×10^{-24} e cm.

In the second term of (20), $\delta\overline{v_x}$ is minimized by comparing the Ramsey fringe widths of the up and down beams and adjusting the oven temperatures to equalize these widths to better than 1%. From the difference of up and down asymmetries we

continuously measure $\langle B_y/B_z \rangle$ and maintain this quantity at less than 1×10^{-5} on the average. Thus the second term of (20) contributes less than 3×10^{-25} e cm to d_a.

The third term of (20) is non zero if both beams do not experience the same B_y; this is possible if the two beams do not overlap exactly in y or z <u>and</u> the magnetic fields are inhomogeneous. Two independent techniques have been used to measure this contribution. In the first, a large magnetic field gradient at the beam axis ($\partial B_y/\partial y=2.6\times10^{-3}$ G/cm) is deliberately imposed by means of the four inhomogeneity wires mentioned earlier and the EDM asymmetry is measured. Since the actual gradient with no inhomogeneity wire current is measured to be less than 1×10^{-5} G/cm (see discussion below), the result obtained for the EDM can be reduced by the corresponding ratio. The result is a contribution to d_a of less than 4×10^{-25} e cm.

Next consider the second method. The quantity:

$$\frac{\delta B_y}{\langle B_z \rangle} = \frac{\frac{\partial B_y}{\partial z}\delta z + \frac{\partial B_y}{\partial y}\delta y}{\langle B_z \rangle} \tag{21}$$

appears in the third term of (20), where δy and δz are the mean relative displacements of the up and down beams in the y and z directions respectively. In this method we measure independently all four quantities appearing in the numerator of the right hand side of (21). Since $\nabla \mathbf{x} \mathbf{B} = 0$, we have $\partial B_y/\partial z = \partial B_z/\partial y$. The latter quantity is measured by employing an atomic beam that is very small in the y direction, scanning it over the y dimension Δy = .5 cm of the complete beam, and measuring the frequency shift:

$$\Delta \nu = \frac{\gamma}{B_z}\frac{\partial B_z}{\partial y}\Delta y \tag{22}$$

This yields $|\partial B_y/\partial z| \leq 3.6\times10^{-6}$ G/cm. To measure δz we impose a known $\partial B_z/\partial z$ with the four inhomogeneity wires and determine the resulting frequency shift between up and down beams. We find that $\delta z \leq .001$ cm; this taken together with (22) implies that the contribution of the first term on the right hand side of (21) to d_a is less than 6×10^{-26} e cm. As for the second term in (21), the condition $\nabla\cdot\mathbf{B}$ =0 and neglect of x field gradients, which are sufficiently small, permits the approximation $\partial B_y/\partial y \approx -\partial B_z/\partial z$. We then measure the resonant frequency change in either beam as we scan across its z dimension with auxiliary slits. The result is $|\partial B_y/\partial y| \leq 1\times10^{-5}$ G/cm. To measure δy we use two of the inhomogeneity wires to impose a large $\partial B_z/\partial y$ (3.6×10^{-4} G/cm) and again measure the resonant frequency difference between up and down beams. We thus obtain $\delta y \leq .001$ cm. Consequently the second term of (21) contributes less than 1.8×10^{-25} e cm to d_a, and the total contribution, according to the second method, is less than 2.4×10^{-25} e cm, in agreement with the limit imposed by the first method.

The last term in (18) can produce a small E-odd (but B-even) asymmetry if the electric field does not reverse exactly. Periodically during runs we measured the voltages on each electric field plate for each polarity and found them to be less than 3 parts in 10^4. Finally, we note that the Exv effect in this experiment is complementary to the Aharonov-Casher effect observed with neutron interferometry and described by Dr. S. Werner elsewhere in this Conference. Both arise from the same term in the Lagrangian.

4.3 Other Systematics

Charging currents can cause a false EDM in two different ways. First, if the peak electric field charging currents are too large, they may generate magnetic fields that magnetize the magnetic shielding differently for the two electric field polarities. Normally the peak charging current is 1 mA. By taking EDM data with a peak charging current of 400 mA , an upper limit on this contribution to d_a is obtained of 3×10^{-25} e cm.

Charging currents may also generate an EDM-like asymmetry if the plates are not fully charged when data taking begins. This has been checked by changing the timing of the data acquisition so that a delay of only 200 ms is employed before collecting data, and then data is acquired for only 400 ms. This leads to an upper limit on this contribution to d_a of 2×10^{-25} e cm.

Electron emission from one plate to the other or to ground will give rise to a current and a corresponding magnetic field. Since the surface structure of the two plates may differ, the electron emission and therefore the magnetic field may depend on the electric field polarity. A test run at 125 kV/cm with leakage currents 60-200 times larger then in our normal run (where the leakage currents were 10 nA or less) allowed us to set an upper limit on this contribution to d_a of 8×10^{-25} e cm.

In order to avoid a systematic due to computer control signals and groundloops we have only one ground point for the entire apparatus. We have considered other possible sources of systematic effects: phaseshift errors, different velocity distributions, different backgrounds, calibrating sensitivity error, different rf power to the two loops, non-overlapping single-loop resonances, rf frequency off resonance center and the acceleration (deceleration) of the down (up) beam due to gravity. None of these give a significant contribution at our present level of sensitivity. The various systematics are summarized in Table 1.

TABLE 1.

CONTRIBUTIONS TO THE SYSTEMATIC UNCERTAINTY IN d_a (10^{-24} e cm)

Systematic effect	Run I	Run II
Exv:		
Imperfect beam overlap and magnetic field gradients	3.3	0.4
Non-zero v_y and B_x	3.5	1.2
Velocity difference and residual B_y	0.3	0.3
Geometric Phase:	2.4	1.0
Leakage Currents:	0.4	0.8
Charging Currents:		
High Peak	0.3	0.3
Still Flowing	0.2	0.2
Total Systematic Uncertainty*	5.4	1.9

* Calculated by combining individual contributions in quadrature

5. RESULTS

Two separate runs were made. The first was done at a magnetic field of .17 Gauss and E=112 kV/cm, and resulted in 51 data points, corresponding to 22 hours of integration. It yielded $d_a=(-1.1\pm2.5_{stat} \pm 5.4_{syst})\times10^{-24}$ e cm with the statistical uncertainty here as elsewhere at 68% confidence interval. Here, the systematic uncertainty was dominated by contributions due to **Exv** and geometric phase effects.

In the second run the uncertainties due to these effects were reduced, in the latter case by taking data at B_z = .255 G. However the noise was larger and the sensitivity to a possible EDM was decreased because we employed an electric field of 100 kV/cm . With 49 data points, run II resulted in $d_a= (2.1\pm4.6_{stat}\pm1.9_{syst})\times10^{-24}$ e cm, in agreement with our first measurement.

We did a test run at .085 G in order to put a limit on the B-odd geometric phase effect and to determine the magnetic field dependence of any other contributing false effect. All the data taken at the three values of B_z show evidence of a B-even systematic proportional to B_z^{-2}:

$(-35.4\pm8.5_{stat})\times10^{-24}$ e cm at .085 G,

$(-7.6\pm2.8_{stat})\times10^{-24}$ e cm at .17 G,

$(-3.2\pm4.4_{stat})\times10^{-24}$ e cm at .255 G.

We emphasize the most important conclusion: our data give no evidence for an effect that is both B-odd and E-odd. By adding the statistical and systematic uncertainties linearly for each run, and taking the weighted average of the two runs we obtain:

$$d_a=(1.6\pm 5.0)\times 10^{-24} \text{ e cm.} \tag{23}$$

Note that except for the initial automatic rejection based on excessive noise, no rejections or cuts were made, nor were any corrections applied to the original data. Assuming an enhancement factor in the ground state of thallium of -600, result (23) corresponds to an electron EDM of

$$de=(-2.7\pm 8.3)\times 10^{-27} \text{ e cm.} \tag{24}$$

The uncertainty in the electron EDM does not include the theoretical uncertainty of the enhancement factor. This result represents a significant improvement over all previous measurements[13-17].

ACKNOWLEDGEMENTS

We gratefully acknowledge the excellent work of machinist A. Vaynberg, and also wish to thank N. Claytor, Dr. E. Garwin, Dr K. Halbach, D. Hopkins, Prof. D. McColm, N. Larkin, Prof. M. Suzuki, and A. Wydler for their many useful contributions.

This work was supported by the U.S. Department of Energy, under contract DE-AC-76SF00098, through the Lawrence Berkeley Laboratory's Experimental Research and Development Fund Program; and by the Director, Office of Energy Research, Office of Basic Energy Sciences, Chemical Sciences Division; and in part by the Office of High Energy and Nuclear Physics, Division of High Energy Physics and Division of Nuclear Physics.

REFERENCES

a) Present address: Manne Siegbahn Institute, Frescativagen 24, 104 05, Stockholm, Sweden

b) Present address: Salomon Brothers, Inc., 1 New York Plaza, N.Y.,N.Y. 10004

1. S.M. Barr and A. Masiero, Phys. Rev. Lett. **58**, 187, 1987
2. S.M. Barr and A. Zee, Phys. Rev. Lett. **65**,21,1990
3. R.G. Leigh,S. Paban, and R.M. Xu, Univ. of Texas Theory Group Report #27-90,1990
4. W. Bernreuther and M .Suzuki, LBL Report #27985,1990 Revs. Mod. Phys., to be published
5. L.I. Schiff, Phys. Rev. **132**,2194,1963
6. P.G.H. Sandars, Phys.Lett **14**,194,1965
7. P.G.H. Sandars and R. M. Sternheimer, Phys. Rev. **A11**, 473, 1975

8. V.V. Flambaum, Yad. Fiz (Sov J. Nuc Phys) **24**, 383,1976
9. W.R.Johnson, D.S.Guo, M.Idrees, and J.Sapirstein, Phys. Rev. **A 32**,2093, 1985
Phys. Rev. **A 34**, 1043, 1986

10. E.Lindroth, A.M. Martensson-Pendrill, A.Ynnerman, and P.Oster,
J. Phys. **B 22**,2447,1989
11. N.F.Ramsey, Phys. Rev. **76**,996,1949; Science **248**, 1612,1990
12. M.V. Berry, Proc. R. Soc. **A392**, 45,1984
13. S.A. Murthy, D. Krause Jr., Z.L. Li, and L.R. Hunter,
Phys. Rev. Lett. **63**, 965, 1989
14. H. Gould, Phys. Rev. Lett **24** ,1091,1970
15. M.C.Weisskopf, J.P.Carrico, H.Gould, E.Lipworth, and T.S. Stein,
Phys. Rev. Lett. 21, 1645, 1968
16. S.K. Lamoreaux, J.P.Jacobs, B.R.Heckel, F.J.Raab, and E.N.Fortson,
Phys. Rev. Lett. **59**, 2275,1987
17. M.A. Player and P.G.H. Sandars, J. Phys. B., **3**, 1620, 1970

LAWRENCE BERKELEY LABORATORY
UNIVERSITY OF CALIFORNIA
INFORMATION RESOURCES DEPARTMENT
BERKELEY, CALIFORNIA 94720